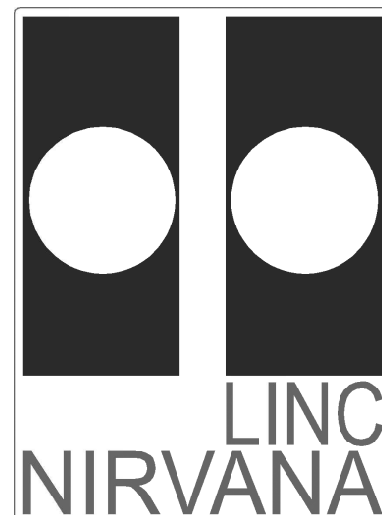


LINC-NIRVANA

The **L**BT **I**nterferometric **C**amera and
Near-**I**nfra**R**ed / **V**isible **A**daptive
interferometer for **A**stronomy

A collaborative project of the MPIA Heidelberg, INAF-Arcetri,
Universität zu Köln, and MPIfR Bonn

<http://www.mpia.de/LINC>



LINC-NIRVANA

—

Design Report of the Fringe and Flexure Tracker Detector

Doc. No. LN-MPIFR-FDR-ELEC-001
Short Title FFTS FDR
Issue 1.1
Date June 6, 2005

Prepared J. Behrend June 6, 2005
Name Date Signature

Approved P. Bizenberger June 6, 2005
Name Date Signature

Released M. Kürster June 6, 2005
Name Date Signature

Document Change Record

Issue	Date	Section/Paragraph Affected	Reasons / Remarks
0.1	June 4, 2004	all	first draft
0.2	July 16, 2004	all	revised issue
0.3	February 16, 2005	all	revised issue
1.0	June 6, 2005	Jan Behrend	revised issue
1.1	June 6, 2005	Jan Behrend	approved issue

Contents

1	Scope	1
2	Applicable Documents	1
3	External Interfaces	1
4	Acronyms	2
5	Introduction	3
6	Requirements	3
6.1	Image and Detector Size	3
6.2	Exposure time and frame rate	3
6.3	Fringe-tracker control loop	3
7	Functions	4
8	Detector	4
8.1	Layout	4
8.2	Specifications	6
8.3	Capability	6
8.3.1	Electronic Gain	6
8.3.2	Conversion factor	7
8.3.3	Readout Noise	7
8.3.4	Photon Transfer Curve	8
8.3.5	Quantum Efficiency (QE)	8
8.3.6	Pixel Properties	8
8.3.7	Dark Current	9
8.3.8	$\frac{1}{f}$ - Noise	9
8.3.9	Pixel bias map	9
8.3.10	Bad pixel map (BPM)	11
8.3.11	Nonlinearity	13
8.3.12	Signal bandwidth of the analog detector output	13
8.3.13	Test results	13
8.3.14	Test frequencies	13
9	Cold Electronics	15
9.1	Detector Mount	15
9.1.1	Detector orientation	15
9.1.2	Cooling requirements	15
9.2	Fanout Board	15
9.2.1	Buffer amplifier	15
9.3	Mechanical mount	16
9.4	Signal Wiring	16
9.4.1	Clock signals and power	16
9.4.2	Analog signals for video, bias and power	16
9.4.3	Temperature sensors	16

10 Warm electronics	17
10.1 Electronics Housing	18
10.1.1 Mechanical Interface	18
10.2 Sequencer	18
10.2.1 Overview	18
10.2.2 Pattern generator architecture	18
10.2.3 Readout Modes	20
10.2.4 Camera Command Interface	20
10.3 Clock driver	21
10.4 Video amplifier	22
10.4.1 Analog video signal processing	22
10.5 ADC and data transmission	22
10.5.1 Reasons for the choice of the ADC	22
10.5.2 Architecture	23
10.5.3 The concept of sub pixel sampling	23
11 Power supply	25
12 Data interface	25
12.1 Requirements	25
12.2 Hardware	25
12.3 Detector Data Interface Box	25
12.3.1 Control Link Serial/F.O. Converter	25
12.3.2 Data Link F.O./Parallel converter	27
12.4 Software	27
A Quantum Efficiency Measurements	29
A.1 Blackbody radiation	29
A.2 Measurement setup	29
A.3 Filter characteristics of the HPF (for thermal background reduction)	30
A.4 Filter characteristics of the K band filter (filter 22)	30
A.5 Blackbody radiation source	31
A.6 Other parameters	31
B Troubleshooting	31
B.1 DMA process cannot find the camera header	31

List of Figures

1	Overview	5
2	Readout electronics	7
3	Detector chip and readout electronics	7
4	Photon transfer curves	8
5	Pixel characteristics	9
6	Dark current image of detector # 170 (ca. 4 min)	10
7	Bad pixels	11
8	Intensity histogram of a single read	12
9	Pixel non-linearity	14
10	Cold electronics on the fanout board	16
11	Wiring scheme	17
12	Scheme of the detector electronics	17
13	Schematic drawing of the sequencer	19
14	Simplified architecture of the pattern generator	19
15	Controlling the LCA	20
16	Programming the LCA	20
17	Signal processing	22
18	Scheme of the ADC	24
19	Sub pixel sampling	25
20	Interface structure	27
21	Shared memory communication	28

List of Tables

1	HAWAII-1 Detector specifications	6
2	Detector #170 measurements	14
3	Power supplies	25
4	Wiring of the Power Supply Rack	26
5	Power supply	26
6	Filters in the aperture wheel of the test dewar	30
7	Wavelength in μm and transmission in % for the K band filter	31

1 Scope

This document describes the LN FFTD subsystem. It is part of the FFTS and records the interferometric images of a reference star in the FOV of the cryogenic interferometric camera.

2 Applicable Documents

No.	Title	Number and Issue
1	Fringe and Flexure Tracking System Hardware	LN-KOELN-FDR-CRY-001 1.0
2	FFTS Detector electronics	LN-MPIFR-FDR-INT-205 1.0
3	CRYOSTAT FFTS electrical Electronic Interface	LN-MPIFR-FDR-INT-208 1.0
4	Cabinets and cabling electrical	LN-MPIFR-FDR-INT-241 1.0
5	COMPUTER FFTS DETECTOR Electrical Interface	LN-MPIFR-FDR-INT-407 1.0

3 External Interfaces

Item	see pages
Mechanical Interfaces	
Detector mount	LN-MPIFR-FDR-INT-205
Filter wheel	
DFE mount	LN-MPIFR-FDR-INT-205
Electrical Interfaces	
Power	25
PCI-DMA board	25
Software Interfaces	
Camera command control	20
Detector image data	27

4 Acronyms

BPM	Bad pixel map
CDS	correlated double sampling
FDDIB	FFTS detector data interface box
DFE	detector front-end electronics
DMA	Direct memory access
DU	digital units
FFTD	Fringe and Flexure Tracker Detector
FFTS	Fringe and Flexure Tracker System
F.O.	fiber optics
FOV	field of view
HPF	High pass filter
HW	Hardware
LBT	Large Binocular Telescope
LCA	Logic cell array
LN	LINC-NIRVANA
LN2	liquid nitrogen
PCI	Peripheral component interconnect
PDR	Preliminary Design Review
PTC	Photon transfer curve
RON	readout noise
SMD	surface mounted device
SW	Software
WS	computer workstation

5 Introduction

The fringe-tracker detector is located inside the LINC-NIRVANA cryostat. The cryostat contains the cryogenic optics, which combines the light coming from the two telescopes in the interferometric focus. A set of selectable dichroic beam splitters reflects the light of a desired band to the science detector, while the other bands can be used for fringe tracking. Additional filters will be used to further select a certain wavelength range. A large FOV of approx. one arcmin square can be used for fringe tracking; the physical size of the image plane is more than 210 mm. The fringe-tracker detector will be moved within the image plane on an xyz translation stage.

6 Requirements

6.1 Image and Detector Size

The F-number of the cryogenic beam combiner optics is $F = 31.8$. A 1-arcmin FOV corresponds to 210.9 mm in the image plane. For fringe tracking, it is sufficient to have a small detector of 32x32 pixels, which can be moved on a translation stage within the large, 1-arcmin FOV. As the detector has to sample the fringes properly as discussed above, the pixel size should be comparable to those of the science detector. A cost-efficient solution is to use a 1-quadrant HAWAII-1 detector with 18.5 micron pixel size for fringe tracking. For a finder function a field of 400x400 pixels is foreseen.

6.2 Exposure time and frame rate

The maximum achievable frame rate (which defines the minimum exposure time) depends on the pixel clock frequency, the image size and additional delays during readout. For a 32x32 field (starting at the first pixel in the row and line) the theoretical time t_R to read the detector is $32 \times 32 \times t_{CLK}$ or roughly 1 ms. In practice, it is advisable to omit the first two rows and lines of the detector. Nevertheless, these pixels have to be read, resulting in a field of 34x34 pixels. The line reset and the overhead needed to advance to the next line take another 6 clock cycles, and the time to prepare the new read is about 24 clock cycles. The total time is $t_R = (34 \cdot (34 + 6) + 24) \cdot t_{CLK}$. In correlated double sampling mode, the maximum frame rate is $1/(2 \cdot t_R)$, and the exposure time therefore is t_R . In the read-reset-read mode, the frame rate is the same as in CDS, but the exposure time is about $2 t_R$. In Burst mode, the frame rate is $\frac{1}{t_R}$ and the exposure time is t_R . The minimum frame rate is 5 Hz.

6.3 Fringe-tracker control loop

The recorded interferometric PSFs contain information about the piston phase difference between the two telescopes. With the calculations shown in equation 6.2 we can determine the framerate t_R

for e.g. CDS using the maximum pixel clock frequency of $f_{p \max} = 2$ MHz:

$$\begin{aligned} f_{p \max} &= 2 \text{ MHz} \\ \Rightarrow t_{CLK} &= 0.5 \mu\text{s} \\ t_R &= (2 \cdot 34 \cdot (34 + 6) + 24) \cdot t_{CLK} \\ \Leftrightarrow &= 1.372 \text{ ms} \\ &\triangleq 728.86\text{Hz} \end{aligned} \tag{1}$$

7 Functions

The system consists of five main components

- Detector
- Cold electronics
- Warm electronics
- Power supply
- Data interface

8 Detector

8.1 Layout

Cable specifications can be found in interface document LN-MPIFR-FDR-INT-407. All parts in drawing 1 are located close to the FFTS WS.

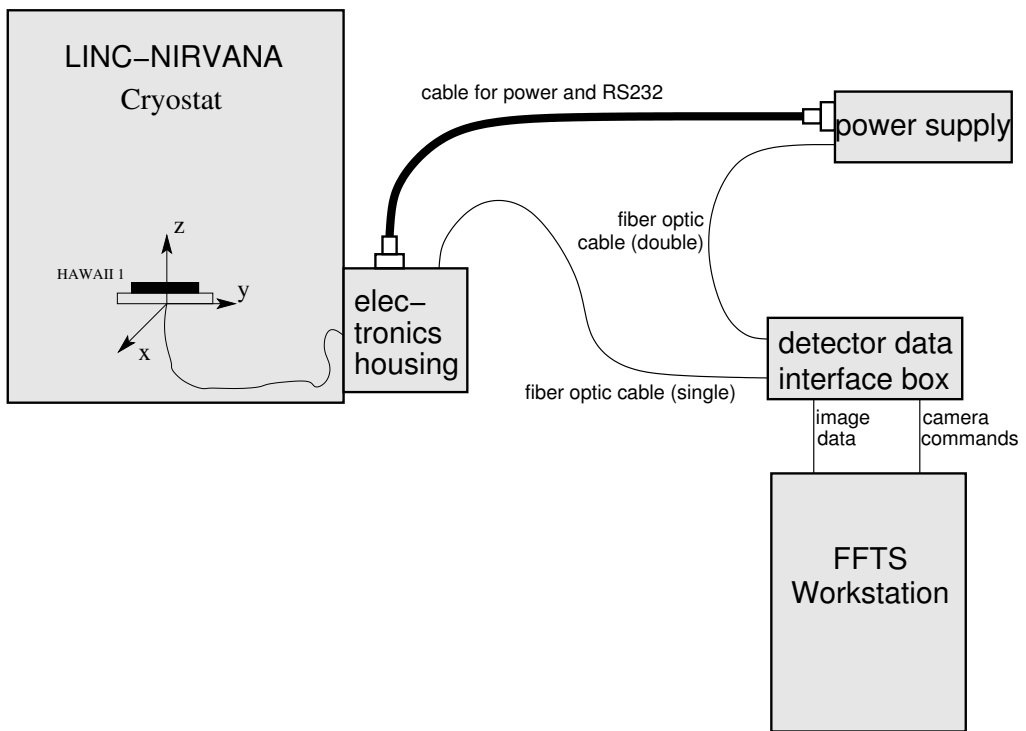


Figure 1: Overview

8.2 Specifications

We will use a one quadrant HAWAII-1 FPA from Rockwell for the FFTS detector. Within the 512x512 pixels of the FPA, a 32x32 pixel field will be read as input for the FFTS control loop. The pixel size is 18.5x18.5 micron, comparable to the science detector. The required image size is 32x32 pixels in K band. As the Airy disk scales down to half the size in J band, a field of 16x16 would then be sufficient. For a finder function, a field of 400x400 pixels is foreseen. The field sizes can be chosen as needed (see sec. 10.2.4)

Table 1: HAWAII-1 Detector specifications

format	1 quadrant of 512 x 512 pixels
wavelength range	1.1 - 2.4 micron
pixel size	18.5 x 18.5 micron
subwindow size	32 x 32 pixels, location freely selectable
pixel-clock frequency	455 kHz up to 2 MHz
readout noise	15 e ⁻ with CDS 455 kHz
frame rate	728 Hz with CDS
detector quantum efficiency	> 50 %
operating temperature	77 K (LN2)

To determine detector characteristics, cold, dark images are needed (see sec. 8.3.6). There must therefore be a filter wheel position which blocks all light.

8.3 Capability

The tests for the detector characterization have to meet certain conditions:

- The detector must be cooled to 77 K.
- The detector electronics has to be warmed up, i.e. must have been running for at least 30 minutes before testing.
- A flatfield is needed to illuminate the detector evenly.
- A cold dark slide inside the dewar is needed to record dark images.

The flatfield is a problematic point in this list, because it is rather hard to illuminate the detector uniformly. Without a good flatfield, the fixed pattern noise is hard to compensate for.

If not otherwise noted, results are taken from measurements with, detector chip # 170.

8.3.1 Electronic Gain

The electronic gain is measured with Y [V] as an input to the fanout board, which is the output of the detector chip, and X [DU] as the output of the analog to digital converter.



Figure 2: Readout electronics

$$\begin{aligned} \frac{X}{Y} &= 116,959 \frac{\text{DU}}{\text{V}} \\ \Leftrightarrow \frac{Y}{X} &= 8.55 \frac{\mu\text{V}}{\text{DU}} \end{aligned} \quad (2)$$

8.3.2 Conversion factor

The conversion factor k is determined by the slope of the linear relation between illumination intensity I of the detector chip and the corresponding temporal variance σ^2 (photon transfer curve (PTC), see 8.3.4 and figure 3). It specifies the number of electrons e^- needed to raise the output of the ADC by 1 DU.

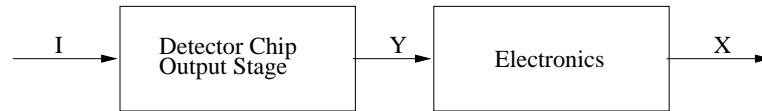


Figure 3: Detector chip and readout electronics

$$k = \frac{I}{X} = 2.11 \frac{e^-}{\text{DU}} \quad (3)$$

Equations 2 and 3 give the following relation:

$$\begin{aligned} \frac{X}{I} \cdot \frac{Y}{X} &= 0.474 \cdot 8.55 \left[\frac{\text{DU} \cdot \mu\text{V}}{e^- \cdot \text{DU}} \right] \\ &= 4.05 \frac{\mu\text{V}}{e^-} = k^* \end{aligned} \quad (4)$$

k^* is called the conversion gain of the detector chip. This parameter is independent of the DFE.

8.3.3 Readout Noise

The readout noise (RON) of the detector chip is determined by taking a number of dark frames and calculating the temporal standard deviation σ_{dark} [DU] over these frames. To yield the noise floor in e^- , this figure is multiplied by the conversion factor k :

$$\begin{aligned} \sigma_{\text{RON}} &= \sigma_{\text{dark}} \cdot k = 7.35 \cdot 2.11 \left[\frac{\text{DU} \cdot e^-}{\text{DU}} \right] \\ &= 15.5 e^- \end{aligned} \quad (5)$$

8.3.4 Photon Transfer Curve

Figure 4 shows the so called photon transfer curves, which express the relation between illumination intensity and temporal variance (noise) of the signal.

When there is almost no illumination, the readout noise dominates the graph. Since readout noise is a characteristic of the FPA, the illumination intensity has to rise above this noise floor before any sensible output can be observed. Once the illumination intensity has reached this level, the output corresponds (almost) linearly to the detected electrons. Above a certain level of intensity the FPA output signal does not reflect the illumination of the detector chip anymore and therefore cannot be used to get image data (see sec. 8.3.11). The left graph in figure 4 shows a schematic of a photon transfer curve, on the right the actual measured curve is displayed.

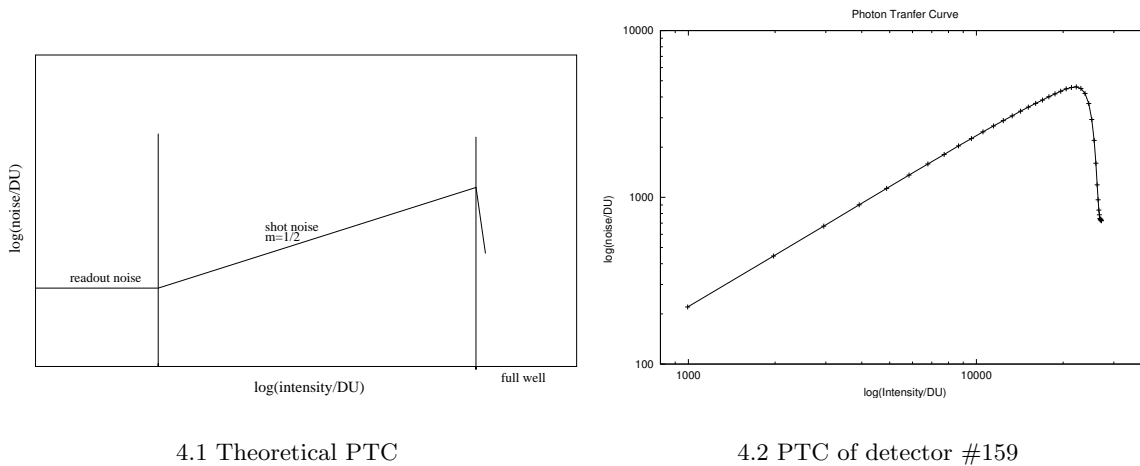


Figure 4: Photon transfer curves

8.3.5 Quantum Efficiency (QE)

Measurement principle The QE is the ratio of the mean number of electrons detected divided by the number of incoming photons. To measure the QE, a blackbody was used as a light source, because the number of emitted photons can be calculated with sufficient precision.

ROCKWELL specifies the QE of their HAWAII detector chip as of 60% in K-band. In our measurements we confirmed this figure.

Appendix A contains a complete description of the measurement setup and the corresponding results.

8.3.6 Pixel Properties

Figure 5 shows the basic detector chip characteristics:

- pixel bias
- pixel gain

- global bias depending on the illumination

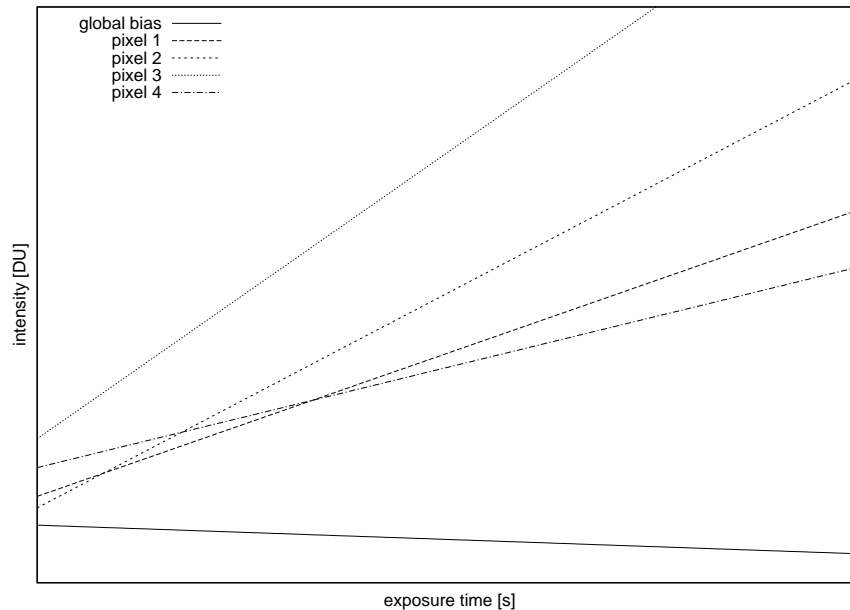


Figure 5: Pixel characteristics

Nonlinearity effects are not shown here (see sec. 8.3.11). As an example, four individual pixels are presented. Each has its own pixel bias and gain. In addition, a global bias must be taken into account while compensating for pixel bias. The more the chip is illuminated, the lower the global bias gets.

To compensate for several of these effects, the detector was prepared with a 30 pixels wide “shadowed column” on the left edge of the FPA (see figure 6).

8.3.7 Dark Current

The dark current is a detector effect which can be observed if the chip is read out with very long exposure times. Although there is no light coming into the dewar, after a few minutes there is an output signal. This is caused by thermal effects such as power dissipation of output stage transistors and readout shift registers. This dark current is shown in figure 6.

8.3.8 $\frac{1}{f}$ – Noise

$\frac{1}{f}$ – Noise is an effect of certain electrical components. With rising frequencies f , this noise effect gets smaller and smaller. This is why this kind of noise is called $\frac{1}{f}$ – Noise. The visible effect in an image is a vertical wave pattern. With the high frame rate of the FFTS detector we do not expect to see $\frac{1}{f}$ noise contributions, as we will be in a frequency range of > 100 Hz.

8.3.9 Pixel bias map

The expected values for double correlated dark images consist of dark current and noise. Because dark current dominates not before several minutes of exposure (at 77K), one would expect that the



Figure 6: Dark current image of detector # 170 (ca. 4 min)

pixel values of double correlated dark images represent only noise, and therefore the mean value should be zero. Real double correlated dark images taken with the FFTS detector system show at least two effects:

1. A vertical ramp over the whole quadrant coming from effects inside the detector.
2. Some pixels show a very high difference value between the first and second read.

Most of the pixels which show very high values are marked as bad, but the electronic effects must be compensated for by using a pixel bias map.

A pixel bias map is only valid for a specific sub-window setup and exposure time. i.e. just before taking scientific data, dark images with the same setup must be recorded. To generate a useful pixel bias map, at least 100 dark images are necessary. The calculation of pixel bias maps uses formula 6.

$$PBM = \frac{1}{N_z} \sum_{i=1}^{N_z} P_i \quad (6)$$

where PBM is the value of a pixel in the pixel bias map, N_z is the number of dark images, P_i is the pixel value from the i^{th} image.

8.3.10 Bad pixel map (BPM)

The process of bad pixel map generation uses three criteria:

1. The noise behavior of a pixel is used for a preliminary bad pixel map.
2. A model for an ideal, pixel based on the photon transfer curve, is used for creating the final bad pixel map.
3. A sensible limitation of the conversion factor.

The reason for using the noise behavior is that this criteria can be used for the whole quadrant, and not just for the illuminated part of the detector.

An example of bad pixels because of noise can be seen in figure 7. On the left, a portion of a dark image of the detector is shown. No anomalies can be detected. Nevertheless, compared to the rest the variance of certain pixels is much higher as shown on the right.

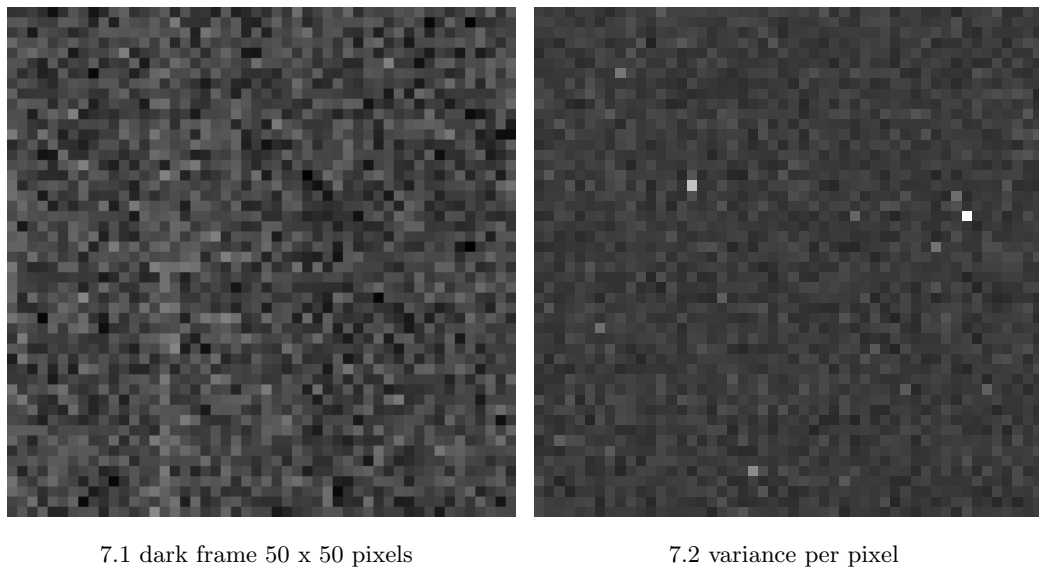


Figure 7: Bad pixels

The reason for using the photon transfer curve is that we can calculate the photon transfer curve for each individual pixel, and this curve is not dependent on the homogeneity of the illumination. The values for the slope of an ideal pixel is exactly 0.5, which can be used for the decision if a pixel is useful or not.

Another criteria is the pixel bias. If it is too high, the dynamic range of this pixel is compromised. Figure 8 shows the histogram of a dark single read of the detector. It shows a number of pixels which have a higher bias than the others. Where to put the line to distinguish between “good” and “bad” is a matter of the required quality of the resulting images.

The generation of a preliminary bad pixel map uses a series of dark images. For each pixel, the mean value and the variance is calculated (see equation 7 and 8).

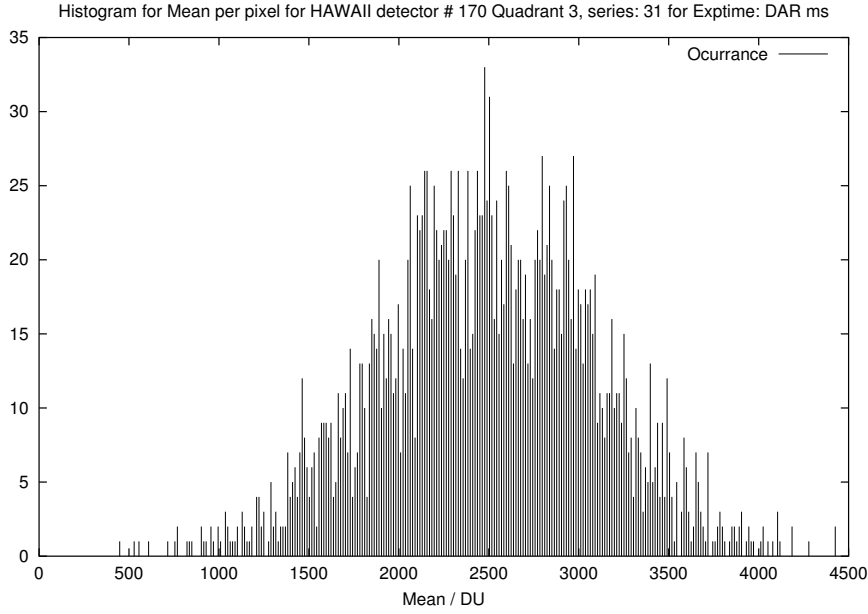


Figure 8: Intensity histogram of a single read

$$m = \frac{1}{N_z} \sum_{i=1}^{N_z} P_i \quad (7)$$

$$\sigma^2 = \frac{1}{N_z - 1} \sum_{i=1}^{N_z} (P_i - m)^2, \quad (8)$$

where m is the average intensity and σ^2 is the variance over time of a pixel. N_z is the number of dark images, P_i is the pixel value from the i^{th} image. Based on these values, equation 9 is used to define whether pixels in the preliminary bad pixel map are useful or not.

$$BPM = \begin{cases} 0 & : \sigma^2 > L \\ 1 & : \sigma^2 < L \end{cases} \quad (9)$$

Where BPM is the value in the preliminary bad pixel map and L is the limit for the variance (42.0 for example).

The generation of a final bad pixel map uses a generated photon transfer curve map (see chapter 8.3.4). For bad pixel map generation, only the slope of the PTC and the quality, i.e. squared relative error divided by the number of data points, is necessary. Because the generation of photon transfer curves uses the preliminary bad pixel map, no final bad pixel map is needed before this map is generated. Based on the photon transfer curve, equation 10 is used to distinguish between useful and useless pixels.

$$BPM = \begin{cases} 0 & : (a_1 < L_1) \vee (a_1 > L_2) \vee (q > L_3) \\ 1 & : (a_1 > L_1) \wedge (a_1 < L_2) \wedge (q < L_3) \end{cases} \quad (10)$$

Where a_1 is the slope of the photon transfer curve of a pixel, q is the quality of the fit, i.e. squared relative error divided by the number of data points, L_1 is the smallest allowed slope, L_2 is the largest allowed slope and L_3 is the minimal required quality.

8.3.11 Nonlinearity

The analog output signal of the detector is not a linear function of the pixel charge accumulated during the exposure time. Nonlinearity already begins at medium signal levels. For example, at signal levels of 50% of the full well capacity, a nonlinearity of more than 1% is typical. The nonlinearity increases with higher full well capacity. For the LN FFTS detector, a nonlinearity of a few percent is still acceptable, due to the fact that the fringe position has to be correct, but not the fringe contrast. This means that we can extend the useful dynamic range to higher signal levels. The acceptable nonlinearity could be as high as 5%. However, we developed a method for nonlinearity compensation, which allows us to increase the dynamic range to 80-90% of the full well capacity.

We use a physically reasonable model to compensate one nonlinear effect in order to extend the useful dynamic range of a detector up to 90% of the saturation level of an individual pixel. This model assumes that the capacity of a pixel depends on the already accumulated charge of that pixel. Due to the simplicity of the model, the saturation effect is ignored. The model is represented by formula 11.

$$U = \frac{Q}{C_0 + \alpha Q}, \quad (11)$$

where U is the measured voltage, Q is the accumulated charge and C_0 the capacity of an empty pixel. For practical reasons, formula 12 is used to model flatfield and nonlinear properties of a pixel:

$$I_R = \frac{aI_C}{1 + bI_C} \quad (12)$$

Where I_R is the measured raw intensity, I_C the calibrated intensity, a the relative gain and b the nonlinearity factor.

A nonlinearity map contains three values for each pixel. One value defines a limit up to which the nonlinear behavior can be compensated (e.g. modelled by equation 12). The other two values define parameters a and b from equation 12. In Figure 9 shows that for the flatfield compensation, the non-linearity exceeds the $\pm 0.5\%$ limit at about 19000 DU. If the non-linearity is compensated by the inverse of Eq. 12, the useful dynamic range extends to 26000 DU.

8.3.12 Signal bandwidth of the analog detector output

The analog bandwidth of the detector output shows a low pass characteristics with a cutoff frequency of about 1 MHz. The detector can operate at 2 MHz, but with a gain drop of about 6 dB. Although this is unacceptable for normal operation, since it reduces the signal-to-noise ratio dramatically, this clock speed could in principle be applied for bright objects.

8.3.13 Test results

Table 2 shows the test results for detector # 170

8.3.14 Test frequencies

The BPM must be regenerated after each cool-down. The pixel bias map depends on the timing of the detector readout. Therefore, if any readout parameter like subarray size or location, exposure

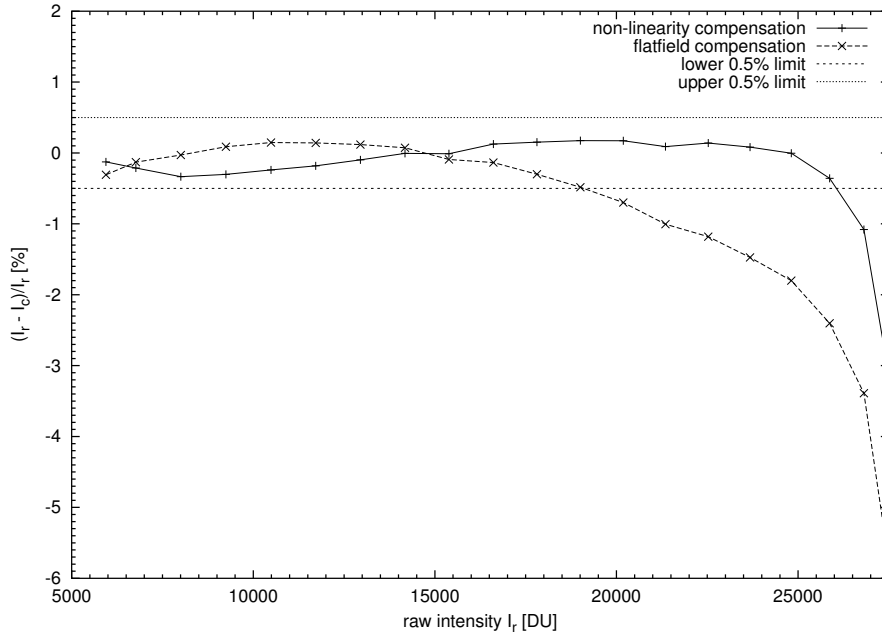


Figure 9: Pixel non-linearity

Table 2: Detector #170 measurements

RON (double correlated)	15.5 e ⁻ @ 450 kHz, 30 e ⁻ @ 1 MHz
RON detector electronics	2 e ⁻
conversion factor	2.11 $\frac{e^-}{DU}$
full well capacity	≈ 110,000 e ⁻ @ $U_{\text{reset}} = 0.5$ V
1 % nonlinearity	≈ 39,000 e ⁻ , uncorrected
1 % nonlinearity	≈ 90,000 e ⁻ , corrected
number of bad pixels	1304 (whole quadrant)
clusters of bad pixels (≥ 4)	≈ 25 (whole quadrant)
CDS frame rate (32 x32 pixel field)	320 Hz

time, etc. is changed, the corresponding pixel bias map (and flatfield map if needed) must be recorded as well.

9 Cold Electronics

9.1 Detector Mount

9.1.1 Detector orientation

Readout Direction (fast, slow) For the readout, the individual detector pixels are selected by activating the horizontal and the vertical shift registers. As the horizontal shift register is faster than the vertical shift register, the detector should be oriented such that the fast direction is parallel to the fringe stripes. This has the additional advantage that even for very fast readout with an increasing crosstalk between consecutive pixels in the readout direction (due to the limited bandwidth of the detector output), the fringe positions will not be affected.

9.1.2 Cooling requirements

The detector operating temperature is 77-80 K. The heat dissipation from the HAWAII-1 array during normal operation is negligible (≈ 1 mW). The main contribution of 0.5 W comes from the operational amplifiers, which drive the differential video signal into the coax cables of 50Ω impedance. In addition, the wire connectins for the clock, video, and power, will add some 0.2 W. The total heat of 0.7 W has to be transported to the cold shields in order to avoid a temperature increase and thus thermal background radiation inside the dewar. The cooled dewar temperature is 60 K. The temperature difference in relation to the detector mount is therefore 20 K. We can now calculate the crosssection of the cooling straps necessary to transport the the heat of 0.7 W to the dewar cold plates. The required cooling power P is:

$$P = \frac{\lambda \cdot A \cdot \Delta T}{l} \left[\frac{\text{W}}{\text{m} \cdot \text{K}} \cdot \frac{\text{m}^2 \cdot \text{K}}{\text{m}} \right] \quad (13)$$

with heat conductivity λ , cross section A , and temperature difference ΔT . For copper, the heat conductivity is $\lambda = 398 \frac{\text{W}}{\text{K} \cdot \text{m}}$. The length of the copper strap is 0.5 m at maximum. For $\Delta T = 20\text{K}$ the resulting cross section of the cooling strap(s) is about 50 mm^2 . In order to keep the detector temperature within the range of 77...80K the detector mount must be heated and the temperature controlled.

For further reading also consult LN-KOELN-FDR-INT-231.

9.2 Fanout Board

The fanout board holds the HAWAII-1 FFTS detector in a socket and supplies it with all necessary clock signals and voltages. All electronic components on the board will be operated at LN2 temperature (77K). Almost no surface mounted devices are used to avoid mechanical tension during cool down and warm up. Capacitors with linear dielectric are used to minimize capacitance degradation in the cold.

9.2.1 Buffer amplifier

The detector output impedance of $10 \text{ k}\Omega$ is too high and the cable length to the outside of 1.5 m is too long to transmit a 5 MHz video signal without preamplification. Therefore, an active amplification

stage is on the fanout board (or if necessary beside it). Operational amplifiers with FET inputs are used to build up a differential signal and to drive 50 Ω transmission lines. The operational amplifiers use a separate cooling strap to drain 0.5 W of thermal heat dissipation. These straps are internally connected to copper blocks, which are in turn connected to the outside cooling straps.

For further reading also consult LN-KOELN-FDR-INT-231.

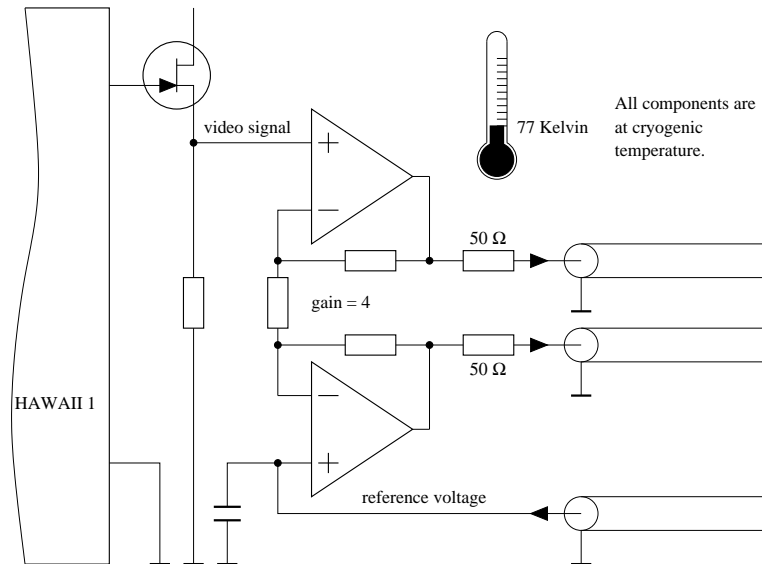


Figure 10: Cold electronics on the fanout board

9.3 Mechanical mount

Please see interface documents LN-MPIFR-FDR-INT-205 and LN-MPIFR-FDR-INT-232.

9.4 Signal Wiring

Clock signals are transmitted to the fanout board using twisted pair lines, which are terminated at the far end. Power supply and bias voltages are driven by C-stable high bandwidth drivers. This ensures voltage stability even for hard load current changes. See figure 11.

9.4.1 Clock signals and power

Please see interface document LN-MPIFR-FDR-INT-205.

9.4.2 Analog signals for video, bias and power

Please see interface document LN-MPIFR-FDR-INT-205.

9.4.3 Temperature sensors

Please see interface document LN-MPIFR-FDR-INT-208.

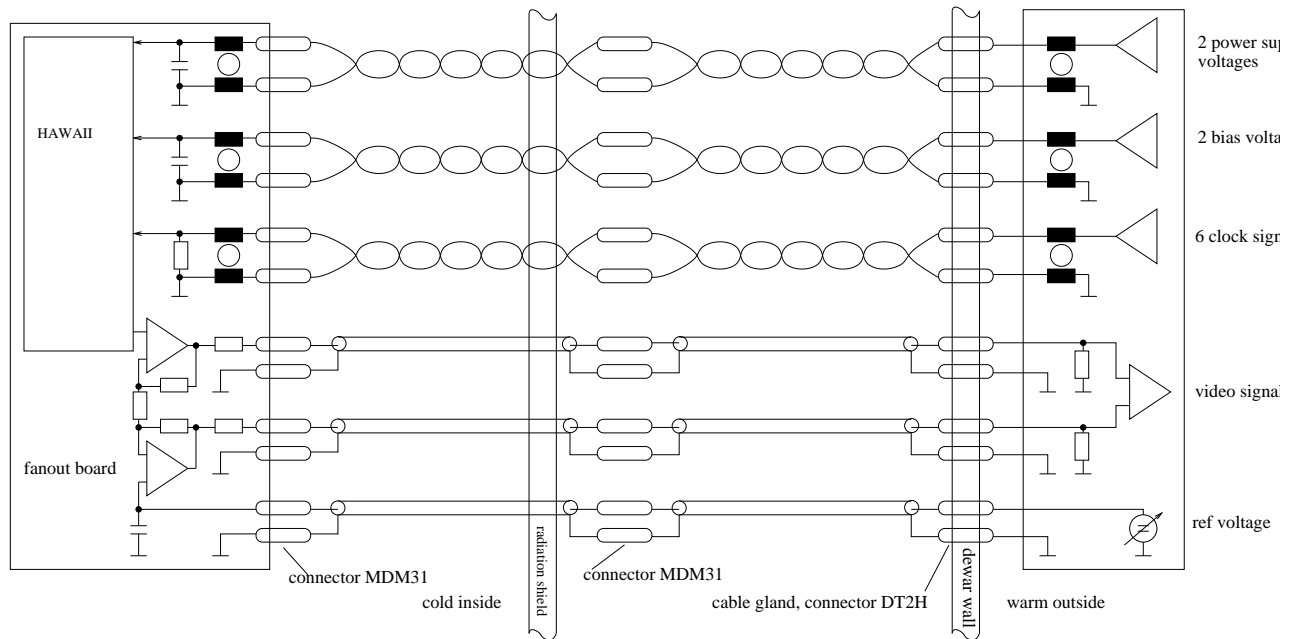


Figure 11: Wiring scheme

10 Warm electronics

The warm electronics consists of the following modules (see Figure 12):

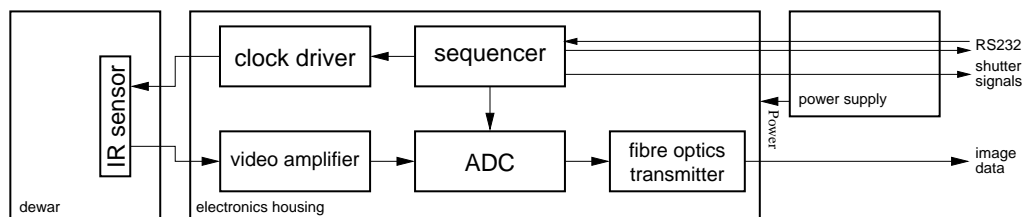


Figure 12: Scheme of the detector electronics

1. A **sequencer** generates the patterns necessary for reading and sampling the IR sensor. It can be configured with a (galvanically isolated) serial line (RS232). It also generates a header containing information about image format, read mode etc..
2. A **clock driver** boosts the digital signals from the sequencer.
3. A **video amplifier** supplies all necessary bias voltages and prepares analog signals from the IR sensor for sampling.
4. An **ADC** samples the analog signal. On the ADC board there are also digital logic sections for averaging several samples (sub pixel sampling, see 10.5.3).
5. A **fiber optical transmitter** feeds the image data into a fiber optic line connected to the detector FFTS WS.
6. A **power supply**, see Sec.11 .

10.1 Electronics Housing

10.1.1 Mechanical Interface

Please see interface document LN-MPIFR-FDR-INT-205.

10.2 Sequencer

10.2.1 Overview

The sequencer generates all necessary clock signals to operate the detector and the sample timing of the ADCs. It also provides Shutter control signals and header information for each frame. The sequencer also supplies a galvanically decoupled RS232 interface for external control. Basically, the sequencer consists of two main units. A logic cell array (LCA) which generates the fast digital signals for one detector readout, and a microcontroller, which is responsible for programming the LCA, doing the timing between readouts and generating the header information. A special challenge concerning the FFTS was to speed up the data rate as much as possible to afford a sufficient sample rate to the control loop. There are several different readout modes implemented, such as correlated double sampling(CDS) and sampling up the ramp with multiple readout (Fowler sampling).

Components Overview:

1. Microcontroller which
 - (a) supplies a command set for configuring the operation mode via RS232
 - (b) generates “slow” digital signals
 - (c) programs the LCA
2. RAM for the microcontroller
3. ROM containing the program code of the microcontroller
4. LCA, which generates “fast” digital signals
5. serial EEPROM, which contains the boot configuration for the LCA. It does not contain any timing, but rather provides the necessary architecture of the LCA. The Microcontroller will supply timing by accessing registers and RAM cells inside the LCA.

10.2.2 Pattern generator architecture

The concept of nested RAM makes use of the fact that patterns for reading an image sensor consist of periodically repeated sequences of simple patterns: Figure 14 shows a schematic diagram of the architecture used for the sequencer. The drawing is simplified, e.g. it is not shown that the clock frequency can vary with every sequence and can be switched between several types of pixels like valid and fast pixels. The smallest pattern is one sample. A sequence of several samples forms one pixel. A repeated number of uniform pixels is called one sequence. One line consists of several sequences. A repeated number of uniform lines is called one area. One frame consists of several areas.

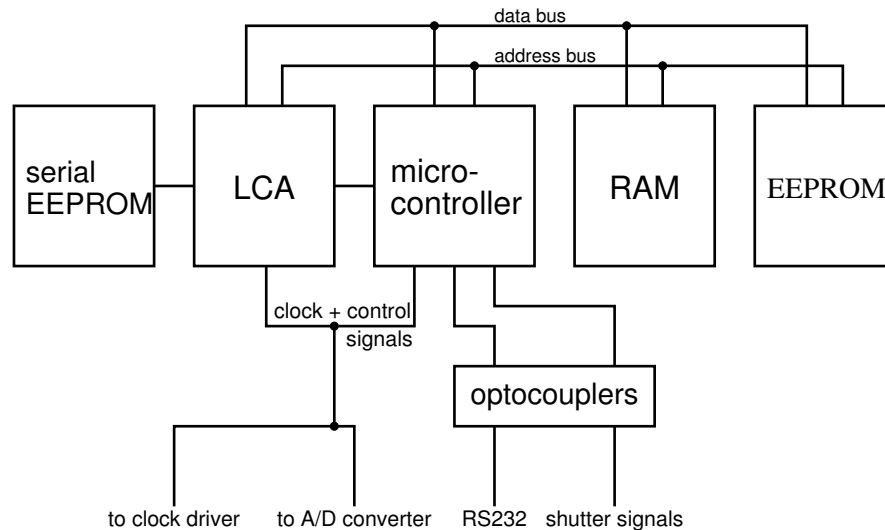


Figure 13: Schematic drawing of the sequencer

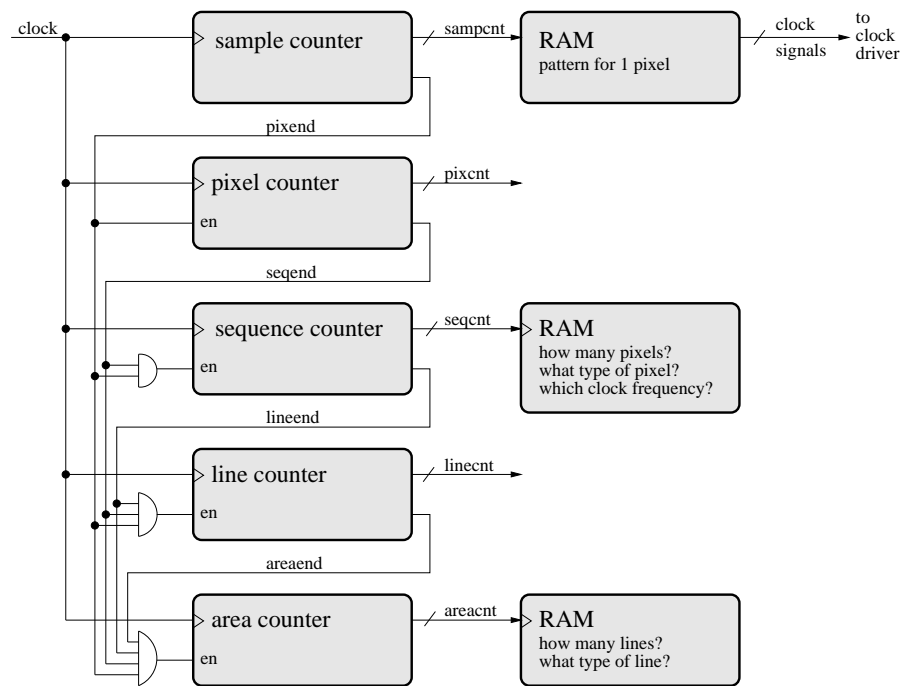


Figure 14: Simplified architecture of the pattern generator

Interaction between microcontroller and LCA After power up, the LCA is configured using a serial EEPROM, as suggested by Xilinx. After configuration, the RAM cells described above appear in the address space of the microcontroller.

Whenever one frame is finished, the LCA activates the signal *picend* (see figure 15). This makes the microcontroller generate an interrupt and disable the clock enable line *clken* to the LCA. Then, the LCA is stopped. After the exposure time interval, it will activate the *clken* line again and the LCA will generate the next readout.

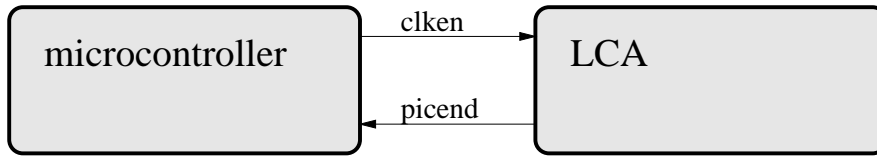


Figure 15: Controlling the LCA

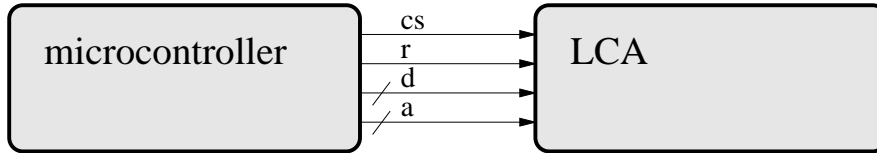


Figure 16: Programming the LCA

10.2.3 Readout Modes

Correlated Double Sampling (CDS): The detector readout sequence is: read1-exposure-read2, where read2 is a destructive read. The final image is the difference between read1 and read2. Advantages: This mode is simple and very stable. It needs the least calibration. It gives a low readout noise. Disadvantage: For the time equivalent to read2, the detector cannot accumulate photoelectrons.

Burst mode: In this mode, multiple reads are taken during the exposure time. The readout sequence is: read1-exposure-read2-exposure-...-readn where readn is a destructive read. The difference between two consecutive reads gives the new image. This mode can be used for low fluxes, where even a large number of exposures (for example 10 or 20) does not saturate the detector. Advantages: The readout noise is comparable to (or even better than) the CDS. The exposure time is the time it takes to read the detector once. The overhead (time where the detector cannot accumulate photoelectrons) is very small ($1/n$). Disadvantages: The last (destructive) read cannot be combined with the first read of the next sequence of reads, so one image is missing and there is not a continuous uninterrupted data stream. The last (destructive) read has a DC offset different to the previous reads (needs additional calibration).

Because the last read is destructive, both Burst and Correlated Double Sampling Mode have an idle mode with reset reads only. This internal mode does not produce any data.

Read-Reset-Read: In this mode, one line of the detector is read as the first step. It belongs to the second read of the previous image. Then, the complete line is reset within one clock cycle. The line is then read again. This read belongs to the first read of the next image. After completing all the detector lines within the selected image area, the readout can start again with the first line. Advantages: No photons are lost, because the new exposure starts directly after the reset. Disadvantages: There is no clear temporal separation between the first and the second read, because they are interweaved. The RON will increase as the first read is taken directly after the line reset.

10.2.4 Camera Command Interface

The following table contains the camera command set for the FFTS.

command	read/write	values	comment
header	RW	on, off	This keyword enables or disables the header, which is sent before the image data.
headtype	RW	long, short	This keyword specifies the type (length) of the header.
state	R	running stopped	Get the current state of the camera.
start	W	none	Start the camera.
stop	W	none	Stop the camera.
exptime	RW	integer	The time between two reads of the same pixel. The unit of exptime is microseconds.
readtime	R	real	The time for one read. The unit is microseconds.
xoffset	RW	integer	The offset in x-dimension. The unit of xoffset is pixels (columns). Only even values are allowed.
yoffset	RW	integer	The offset in y-dimension. The unit of yoffset is lines. Only even values are allowed.
xtotal	RW	integer	The x-dimension of the frame. Only even values are allowed.
ytotal	RW	integer	The y-dimension of the frame. Only even values are allowed.
data	W	none	The camera sends the image through the data link to the LCU. The image size is 8*8 pixels (in uncorrelated readout mode) and the image content is (shifted 1 and 0 bit): 0001 0002 0004 0008 0010 0020 0040 0080 0100 0200 0400 0800 1000 2000 4000 8000 0001 0002 0004 0008 0010 0020 0040 0080 0100 0200 0400 0800 1000 2000 4000 8000 fffe fffd fffb fff7 ffef ffd ffbf ff7f feff fdff fbff f7ff efff dfff bfff 7fff fffe fffd fffb fff7 ffef ffd ffbf ff7f feff fdff fbff f7ff efff dfff bfff 7fff
pixtime	RW	integer	The timing for one pixel: up to 2 MHz
nreads	RW	integer	The number of non-destructiv reads. Valid values are [1 .. 99]
tailrst	RW	on, off	This keyword enables or disables the reset of the part of the detector which is not read.

10.3 Clock driver

The clock driver prepares the digital signals coming from the sequencer and going to the infrared sensor.

We use Elantec MOSFET drivers EL7212 for all clock signals. Each detector supply and bias voltage is individually buffered. All lines going to the detector fanout board inside the dewar are protected against over/under voltage.

10.4 Video amplifier

10.4.1 Analog video signal processing

Outside the dewar, the video signal has to be processed before being converted into a digital data stream (see fig. 17).

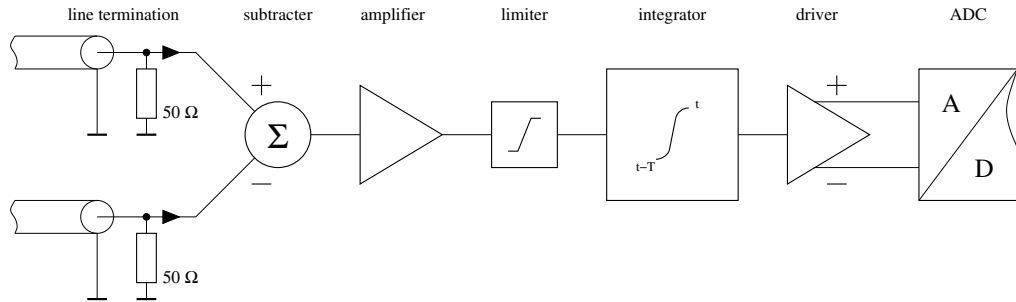


Figure 17: Signal processing

A moving average filter is used to reduce noise. The output of the filter is a continuous signal which is proportional to the average of the input during the past 100 nanoseconds. This time is equal to the sampling period of the ADC.

The filter can mathematically be described as integrator:

$$f_{\text{out}}(t) = \frac{1}{T} \int_{t-T}^t f_{\text{in}}(t) dt \quad (14)$$

$$T = 100 \text{ ns} \quad (15)$$

The practical realization is a purely analog approximation of the integrator. Therefore neither gate-time jitter nor digital clocks can interfere with the signal.

This analog filter is part of a filtering method which is continued on the digital side.

10.5 ADC and data transmission

10.5.1 Reasons for the choice of the ADC

The 14 bit/10 MHz ADC of type AD9240 from Analog Devices and the 16 bit/2 MHz ADC of the type ADC4322 from Analogic seem to be the best choices (as of February 2000). There are no 16 bit converters with a sampling rate greater than 2.5 MHz available.

ADC	AD9240	ADC4322
spurious free dynamic range @ 1 MHz	90 dB typ.	≈ 86 dB
spurious free dynamic range @ 500kHz	90 dB typ.	≈ 98 dB
total power consumption	0.285 W typ.	2.3 W typ.

At low input frequencies the ADC4322 has excellent performance, but it has some other disadvantages which are not easy to quantify:

1. If there are faster infrared sensors available in the future (as already announced by Rockwell) a design with the AD9240 will be easily extendable because, it provides good quality at 10MHz, as well, while the AD4322 will then limit the system performance.
2. The power consumption of the AD4322 is much higher than that of the AD9240.
3. The AD4322 comes in a large package (40 mm by 60 mm) while the AD9240 is available in a PQFP44 package. The electrical quality of the SMD package is superior to the AD4322 package.
4. The AD4322 does not provide differential inputs. This would lead to much worse immunity from electromagnetic interference with the AD4322.
5. The existing MPIFR system already works well with an AD9240. The immunity from electromagnetic interference has proved to be good.

10.5.2 Architecture

The ADC (see figure 18):

1. samples the analog input signal at a constant sampling rate of 10 MHz with 14 bit resolution
2. adds up the 14 bit samples and averages them to a 16 bit output
3. multiplexes 4 channels, and is thus capable of reading a 4 quadrant sensor (not required for LINC-NIRVANA)
4. multiplexes header information into the image data stream

10.5.3 The concept of sub pixel sampling

The moving average filter bandwidth is matched to the ADC sampling speed. By simply adding individual ADC samples, the resulting bandwidth B is inversely proportional to the number of samples, multiplied by T :

$$B = \frac{k}{\text{number of samples} \cdot T}, \quad (16)$$

with $k \approx 1.05$, considering the imperfect analog approximation of the integrator.

After a pixel has been addressed, it takes some time for the analog signal to settle. When the signal is stable, it is sampled several times by an ADC (see figure 19). This so called *sub pixel sampling* has several advantages:

1. Noise can be reduced by averaging the samples taken within one pixel.
2. Since the sample rate is constant, the analog signal acquisition is optimally adapted to the ADC at any pixel rate.
3. The effective signal bandwidth is adapted to the pixel clock frequency by simply changing the number of samples.

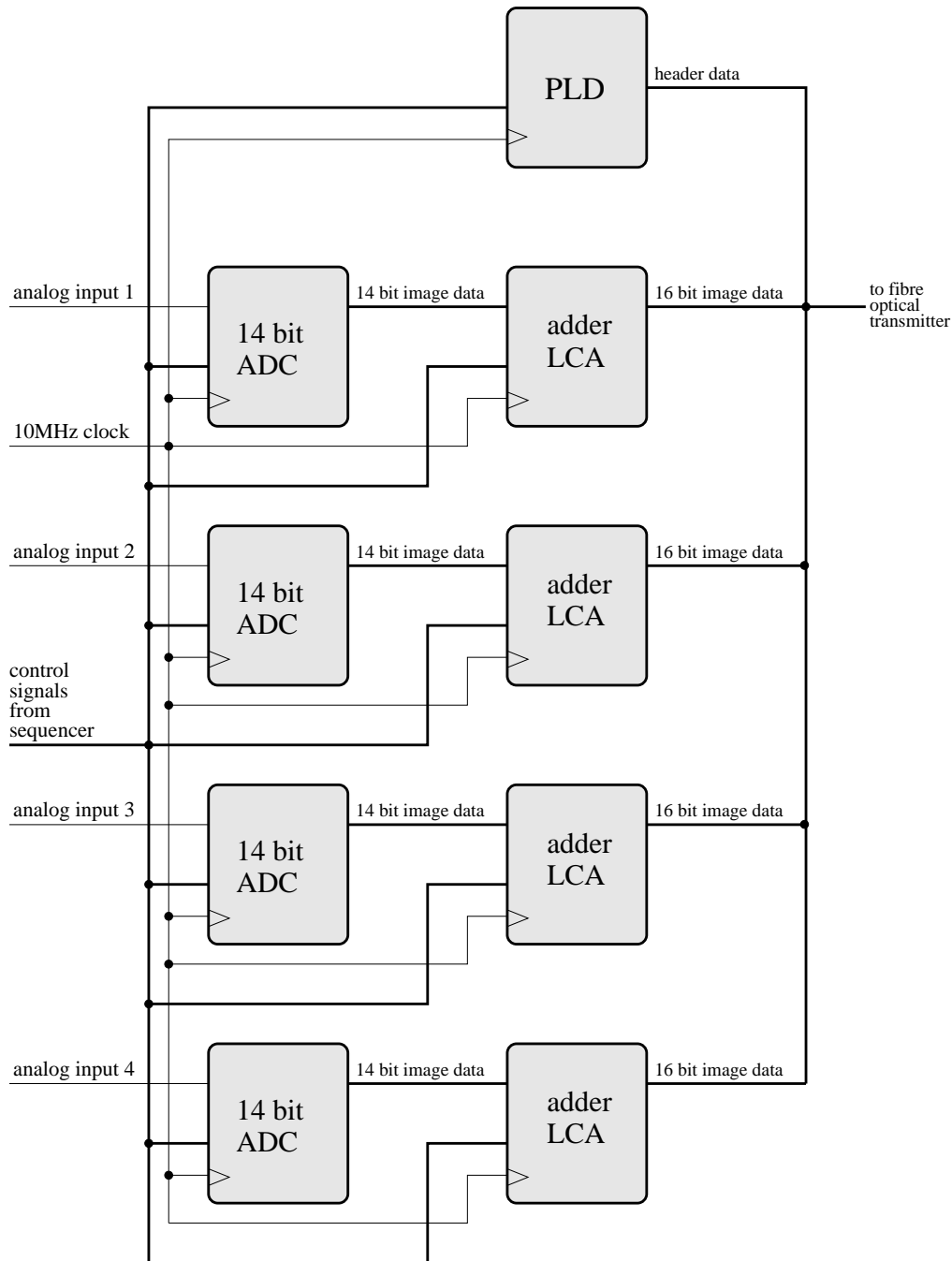


Figure 18: Scheme of the ADC

Fiber optics transmitter (TAXI transmitter) is a part of the ADC board and

1. conforms to the ANSI X3T9.5 standard (aka FDDI, TAXI).
2. converts the 16 bit image/header data stream into a single serial data stream.
3. contains a driver for a fiber optic cable.
4. can handle data rates of up to 6.6 MByte/sec.

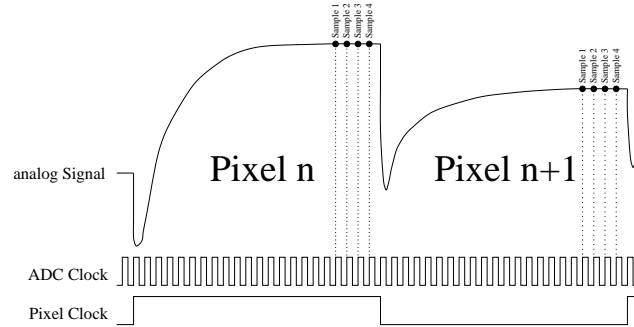


Figure 19: Sub pixel sampling

11 Power supply

The following power supplies are needed. All devices are manufactured by the “KNIEL” company. For further information please see interface document LN-MPIFR-FDR-INT-241.

Type	ANr.	Primary	Secondary
CDÜ 5.1,5 linear	122-004-02	110 V \pm 10%, 40-66 Hz	2x 5 V, 1.5 A
CQ 37 linear	140-045-02	110 V \pm 10%, 0.6 A, 40-66 Hz	4x 8 V
CD 12.1 linear	120-008-02	110 V \pm 10%, 0.4 A, 40-66 Hz	2x 12 V, 1 A

Table 3: Power supplies

12 Data interface

The basic functional structure appears in Fig. 20. Data coming from the camera are acquired by a receive process using a PCI DMA board, putting the data into shared memory which is then accessed by the control-loop process to gain a new set of input data. This is sent to the OPD control. The detector data interface box converts the optical signals to electrical ones, which can be used by the FFTS WS.

12.1 Requirements

12.2 Hardware

12.3 Detector Data Interface Box

The following power supply (table 5) is needed. This device is manufactured by the “KNIEL” company. See also interface document LN-MPIFR-FDR-INT-241

12.3.1 Control Link Serial/F.O. Converter

For the control connection to the DFE, the commercial RS-232/F.O. converter Dataforce/Burr-Brown part #LDM85-S is used. It is installed close to the FFTS WS and connected to it using a standard

Signal	Pin(Box)	Colour	37-pin MIL (TYP:)	Electronics
Kniel CD12.1				
-A U2	2	black	B	Clock-Driver (GND)
+A U2	5	red	C	Clock-Driver (+12V)
-F U2	8	black	M	Clock-Driver (-Sense/GND)
+F U2	11	red	L	Clock-Driver (+Sense/+12V)
+F U1	14	red	E	Video-Amplifier (+Sense/+12V)
-F U1	17	black	F	Video-Amplifier (-Sense/GND)
+A U1	20	red	A	Video-Amplifier (+12V)
-A U1	23	black	D	Video-Amplifier (GND)
Kniel CQ37				
-A U4	2	blue	U	Video-Amplifier (-8V)
+A U4	5	black	T	Video-Amplifier (GND)
-A U3	8	blue	h	Clock-Driver (-8V)
+A U3	11	black	g	Clock-Driver (GND)
-A U2	14	black		LDM85 (GND) Sub-D Pin
+A U2	17	red		LDM85 (+8V) LINC-NIRVANA
Kniel CD5				
-A U2	2	black	Z	ADC-Taxi (GND)
+A U2	5	red	X	ADC-Taxi (+5V)
-F U2	8	black	b	ADC-Taxi (-Sense/GND)
+F U2	11	red	a	ADC-Taxi (+Sense/+5V)
+F U1	14	red	m	Clock-Driver/Sequencer (+Sense/+5V)
-F U1	17	black	n	Clock-Driver/Sequencer (-Sense/GND)
+A U1	20	red	p	Clock-Driver/Sequencer (+5V)
-A U1	23	black	r	Clock-Driver/Sequencer (GND)
RS232 - subD				
TxD	2	white/black	c	Sequencer (TxD)
RxD	3	red/blue	j	Sequencer (RxD)
TxR/R	5	brown/black	d	Sequencer (TxR/GND)

Table 4: Wiring of the Power Supply Rack

Type	ANr.	Primary	Secondary
CDÜ 5.4 switched		220 V \pm 10%, 40-66 Hz	1x 5 V, 4 A

Table 5: Power supply

RS-232. cable (9-pin to 25-pin Sub-D converter; 9-pin extension cord, length \leq 1.5 m):

- data rate $<$ 100 kBd
- fiber length $<$ 2000 m
- power requirements +5 V DC \pm 5%, I $<$ 130 mA

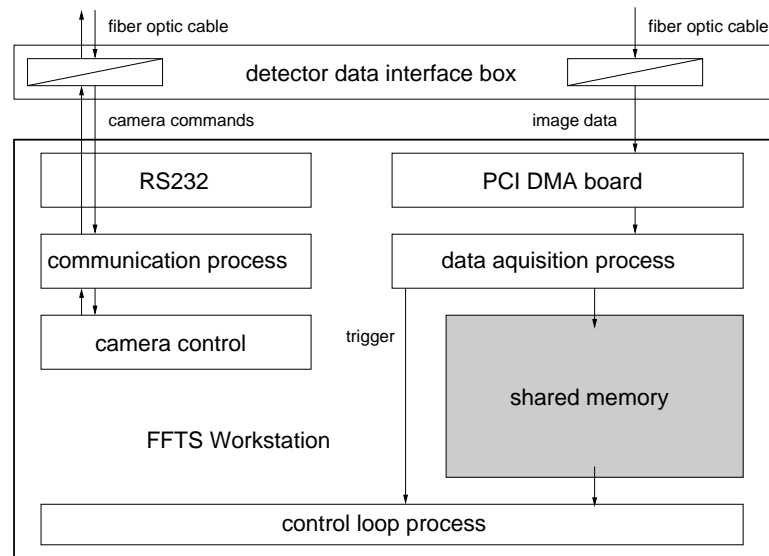


Figure 20: Interface structure

12.3.2 Data Link F.O./Parallel converter

This device was developed by the MPIfR. It converts incoming F.O. data stream to parallel electrical signals, optionally synchronised on frame boundaries, and drives the FFTS WS PCI DMA board.

- input: conforming to ANSI X3T9.5 standard (aka FDDI, TAXI)
- maximum gross data rate: 120 MBit/sec; maximum net data rate: 10.4 MByte/sec
- output drivers: conforming to IEEE 1596.3 SCI LVDS standard
- physical size 200×160 mm, 8 TE wide
- power requirements +5 V DC $\pm 5\%$, $I < 2.5$ A

12.4 Software

Figure 21 shows the basic structure of the software design. It is based on a producer-consumer model accessing a shared memory in which the producer, the data acquisition process, puts the camera data. Then it sends a signal to all the consumers, the FFTS control loop process(es), which then take the data out of the shared memory for further usage. Semaphores are used to keep the processes from accessing data slots at the same time.

For a troubleshooting recipe see B.

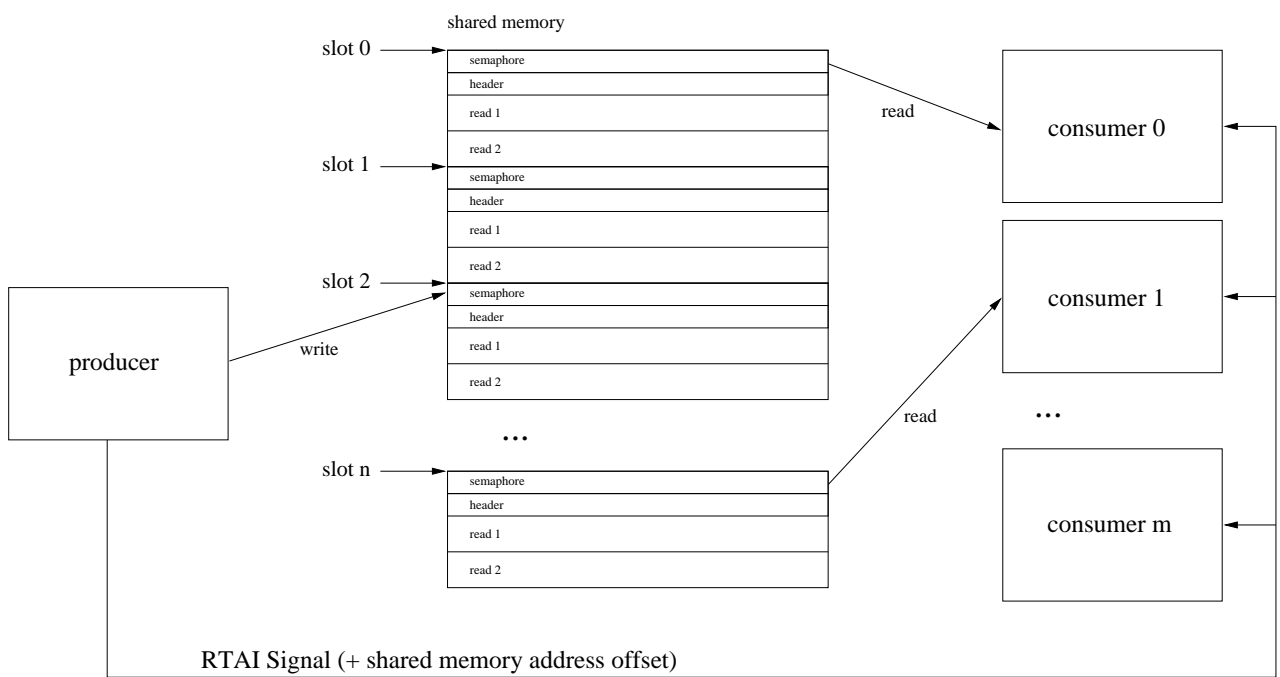


Figure 21: Shared memory communication

A Quantum Efficiency Measurements

For an introductory note see 8.3.5

A.1 Blackbody radiation

From the temperature T of a blackbody, Planck's radiation law determines the quantity of radiation emitted as a function of wavelength. We can calculate the total number of photons $N_{p\lambda}(T)$ emitted by the blackbody per second at temperature T and wavelength λ (per unit area per wavelength interval) by dividing the spectral radiant exitance R_s by the photon energy E_p :

$$R_s = c_1 \lambda^{-5} (e^{\frac{c_2}{\lambda T}} - 1)^{-1} \left[\frac{W}{m^2 \cdot \mu m} \right]$$

$$E_p = \frac{hc}{\lambda}$$

$$N_{p\lambda}(T) = \frac{R_s}{E_p}$$

$$= c_3 \lambda^{-4} (e^{\frac{c_2}{\lambda T}} - 1)^{-1} \left[\frac{\text{photons}}{\text{cm}^2 \cdot \mu m \cdot s} \right]$$

with

$$c_1 = 2\pi hc^2 = 3.74 \cdot 10^8 \left[\frac{W \cdot \mu m^4}{m^2} \right]$$

$$c_2 = \frac{ch}{k} = 1.4388 \cdot 10^4 \left[\mu m \cdot K \right]$$

$$c_3 = 2\pi c \cdot 10^8 = 1.884 \cdot 10^{23} \left[\frac{\text{photons} \cdot \mu m^3}{\text{cm}^2 \cdot s} \right]$$

Finally, the number of photons N_i emitted during the time t [s] into solid angle Ω [sr] from a blackbody (Lambertian emitter) with aperture A_{bb} [cm²] in the wavelength interval $\Delta\lambda$ [μ m] through a filter with transmission $D(\lambda)$ to the detector with tilt ϑ is:

$$N_i = N_{p\lambda}(T) \cdot t \cdot \frac{\Omega}{\pi} \cdot A_{bb} \cdot \Delta\lambda \cdot D(\lambda_i) \cdot \cos(\vartheta) \cdot t_{\text{loss}} \left[\text{photons} \right],$$

where t is the detector integration time.

The solid angle Ω is the pixel area divided by the distance squared between the blackbody and the detector (solid angle definition).

The filter transmission curve $D(\lambda)$ was sampled in small steps of 1 to 10 nm ($= \Delta\lambda$).

ϑ is the detector tilt angle of 6.5°.

t_{loss} is the transmission loss (mainly reflection) of the entrance window (≈ 0.95)

The total number of photons falling on the detector was calculated by numerical integration of N_i over the whole filter wavelength range.

A.2 Measurement setup

A test dewar was put on a table with the orientation of the entrance window to allow the horizontal beam to enter from the blackbody radiation source which was located at some distance. No optics

was used to image the blackbody on the detector. Nevertheless, the blackbody was aligned with the center of the entrance window of the dewar. Different blackbody apertures from 16 mm to 1.5 mm diameter were chosen to adjust the flux. Even the largest aperture was not vignetted by the filter or other geometries inside the dewar, resulting in a well defined radiation area given by the apertures on the blackbody cavity. In addition, the distance from the blackbody to the detector dewar was used as another parameter to vary the flux, as were different blackbody temperatures.

Since the detector is sensitive in the spectral range from 0.8 to 2.5 μm , it could already be saturated for exposure times of a few hundred milliseconds when looking at surfaces at room temperature (≈ 300 K). To avoid this, the narrow K' band filter ($\lambda_c = 2.1\mu\text{m}$, $\Delta\lambda = 200\text{nm}$) installed in the aperture wheel of the test dewar (at 77 K) was selected for the measurements (see table 6). The detector was read with the standard pixel clock frequency of 455 kHz and the parameters: CDS, d1=0, d2=0, exptime=0. The full array with 512 x 512 pixels was read with an exposure time of 580 ms and a sub-array of the inner 128 x 128 pixels with 46.7 ms.

The measurements were performed in three steps:

1. Record the flux from the blackbody (+contamination of the background radiation)
2. Record the background radiation (surrounding surfaces at room temperature)
3. Record dark images (mainly detector readout noise at 77 K) For each measurement 100 images were recorded.

Pos.	Filter-Nr.	Type	λ_c	λ_d
1		HPF	2.3 μm	
2		BLANK	–	–
3	14	J	1.045 μm	4 nm
4	22	K	2.1 μm	200 nm
5		free		
6		free		

Table 6: Filters in the aperture wheel of the test dewar

A.3 Filter characteristics of the HPF (for thermal background reduction)

This high-pass filter has a cutoff wavelength of 2299.9 nm. The transmission is

$< 10^{-2}$ above 2325 nm

$< 10^{-3}$ above 2350 nm

$< 10^{-4}$ from 2355 to 2850 nm

(The detector cutoff wavelength is about 2500 nm, where the QE goes to 0)

A.4 Filter characteristics of the K band filter (filter 22)

Center wavelength: 2.1 μm

Bandwidth (FWHM): 200 nm

See table 7.

1.95	1.96	1.97	1.98	1.99	2.00	2.01	2.02	2.03	2.04	2.05	2.06
0.5	1	2.5	4	10	20	34	51	67	77	80	81
2.07	2.08	2.09	2.10	2.11	2.12	2.13	2.14	2.15	2.16	2.17	2.18
81	81	81	81	80	79	77	76	76	75	76	76
2.19	2.20	2.21	2.22	2.23	2.24	2.25	2.26	2.27			
70	59	35	20	10	4	2	1	0.5			

Table 7: Wavelength in μm and transmission in % for the K band filter

A.5 Blackbody radiation source

Type: CS1050-050 from Electro Optical Industries
 Temperature range: 50 - 1050 °C
 Maximum aperture : 25 mm
 Apertures used: 16 mm, 10 mm, 3 mm, 1.5 mm

A.6 Other parameters

Distance from detector to the outside dewar wall: 75 mm
 Entrance window: CaF_2 of 6 mm thickness
 K band filter thickness: 3 mm
 Blackbody aperture position: 12.2 mm behind the front plate
 Calliper gauge offset: 6.2 mm
 Total distance (detector surface - blackbody aperture)
 $= (75 + 3 + 1.5 + 12.2 + 6.2) \text{ mm} + ds = 97.9 \text{ mm} + ds$

Results can be referred to in section 8.3.5.

B Troubleshooting

B.1 DMA process cannot find the camera header

If the DMA process on the FFTS WS cannot find the camera header, possible reasons are a software failure on the FFTS WS or a hardware failure (e.g. FDE, FDDIB, DMA board or an intermediate connection). The following procedure is recommended in order to solve problems or locate any malfunction. Please have the documents LN-MPIA-FDR-AIT-002 at hand, because it describes how to exchange the FDE, the power supply and the DDIB.

1. Go offline with the software and online again. If the problem persists, continue with step 2.
2. Go offline, power-cycle the FDE by turning off the power supply, wait 10 seconds and switch the power supply on again. Then go online with the software. If the problem persists, continue with step 3.

3. Go offline with the software, open a new terminal window on the FFTS WS and start the test script `fftsTestCamera`. This script executes some tests which check the FDE, the FDDIB, the DMA board and all intermediate connections:
 - (a) The command link between the FFTS WS and the FDE is tested. If there is no valid answer from the camera, all further tests are skipped. This test should be repeated after every action until the script successfully passes all test steps.
 - i. Check the serial connection:
 - Check the cable between the FFTS WS and the FDDIB, exchange the serial cable with the spare one. Rerun the test, if nothing has changed, continue with the next step.
 - Check the serial port on the FFTS WS (hardware) by using a loop back test plug and a terminal program (e.g. `minicom`).
 - ii. Check the FDDIB:
 - Check the power LED. If the LED is off, check the power cord. If everything is ok exchange the FDDIB with the spare one.
 - Swap the two fibers of the serial connection between FDDIB and power supply. If the command link is still not working, swap these two fibers again.
 - iii. Check the power supply:
 - Check the power LED. If the LED is off, check the power chord. If everything is ok, exchange the power supply with the spare one.
 - Check all LEDs on the power supply:
 - If all LEDs are on:
 - * Power-cycle the power supply (restart the FDE).
 - * If the test still fails, exchange the fibers for the serial link between DDIB and power supply with the spare ones (try both combinations).
 - If any LED is off:
 - * Turn the power supply off.
 - * Unplug the thick gray power/RS232 cable on the back of the power supply.
 - * Switch the power supply on again. If any LED is still off exchange the power supply with the spare one.
 - * If all LEDs are on, exchange the thick gray power/RS232 cable establishing the connection between power supply and the FDE.
 - * If the test still fails, exchange the FDE.
 - iv. Exchange the FDDIB.
 - v. Exchange the power supply.
 - vi. Exchange the FDE.
 - vii. Exchange everything in order to cover multiple failures, try both combinations for the fibers from the serial link between DDIB and power supply.
 - (b) All important voltages of the FDE are checked. If one of these voltages is outside of the valid range all further tests are skipped.
 - i. Check the power supply (see 3./(a)/iii.).
 - ii. Exchange the power supply.
 - iii. Exchange the FDE.

- (c) The data link between the FFTS WS and the FDE is tested. This test includes the FDE, the fiber connections, the DDIB, the DMA board and the FFTS WS. If the received pattern is different from the expected pattern all further tests are skipped.
- i. Reboot the FFTS WS and rerun the test.
 - ii. Check the data link:
 - Check the LEDs of the FDDIB (fiber optics link).
 - Power-cycle the FDE.
 - Exchange the data cable between FFTS WS and FDDIB.
 - iii. Exchange the FDDIB.
 - iv. Exchange the DMA board in the FTTS WS.
 - v. Exchange the fiber between FDDIB and FDE with the spare one.
 - vi. Exchange the FDE.